metals

MDPI

Article

Optimal Design of Hot-Dip Galvanized DP Steels via Artificial Neural Networks and Multi-Objective Genetic Optimization

Edgar O. Reséndiz-Flores [1], Gerardo Altamirano-Guerrero [1,*], Patricia S. Costa [2], Antonio E. Salas-Reyes [3], Armando Salinas-Rodríguez [4] and Frank Goodwin [5]

[1] División de Estudios de Posgrado e Investigación, Tecnológico Nacional de México/IT de Saltillo, Blvd. Venustiano Carranza 2400, Col. Tecnológico, Saltillo 25280, Coahuila, Mexico; eresendiz@itsaltillo.edu.mx
[2] Consultores Asociados en Soldadura S.C., Saltillo 25730, Coahuila, Mexico; patricia.costa@consultoresensoldadura.com
[3] Departamento de Ingeniería Metalúrgica, Facultad de Química, UNAM, Circuito de la Investigación Científica S/N, Ciudad Universitaria, Coyoacán, Mexico City 04510, Mexico; enriquesalas@comunidad.unam.mx
[4] Centro de Investigación y de Estudios Avanzados del Instituto Politécnico Nacional, Unidad Saltillo, Av. Industria Metalúrgica 1062, Parque Industrial Saltillo, Ramos Arizpe 25900, Coahuila, Mexico; armando.salinas@cinvestav.edu.mx
[5] International Zinc Association, 2530 Meridian Parkway, Durham, NC 27713, USA; fgoodwin@zinc.org
* Correspondence: galtamirano@itsaltillo.edu.mx

Abstract: This modeling and optimization study applies a non-linear back-propagation artificial neural network, commonly denoted as BPNN, to model the most important mechanical properties such as yield strength (*YS*), ultimate tensile strength (*UTS*) and elongation at fracture (*EL*) during the experimental processing of hot-dip galvanized dual-phase (GDP) steels. Once the non-linear BPNN is properly trained, the most important variables of the continuous galvanizing process, including initial/first cooling rate (*CR1*), holding time at the galvanizing temperature of 460 °C (*tg*) and the final/second cooling rate (*CR2*), are obtained in an optimal way using an evolutionary approach. The experimental development of GDP steels in continuous processing lines with outstanding mechanical properties (550 < *YS* < 750 MPa, 1100 MPa < *UTS* and 10% < *EL*) is possible by using a combined hybrid approach based in BPNN and multi-objective genetic algorithm (GA). The proposed computational method is applied to the specific design of an actual manufacturing process for the first time.

Keywords: DP steels; optimal design; artificial neural networks; multi-objective genetic optimization

Citation: Reséndiz-Flores, E.O.; Altamirano-Guerrero, G.; Costa, P.S.; Salas-Reyes, A.E.; Salinas-Rodríguez, A.; Goodwin, F. Optimal Design of Hot-Dip Galvanized DP Steels via Artificial Neural Networks and Multi-Objective Genetic Optimization. *Metals* **2021**, *11*, 578. https://doi.org/10.3390/met11040578

Academic Editor: Jacek Trzaska

Received: 26 February 2021
Accepted: 29 March 2021
Published: 1 April 2021

1. Introduction

In recent years, the new generation of advanced high-strength steels (AHSS) has been the most affordable mass reduction solution for lightweight vehicles. These steels are the best solution for fuel economy and emission reduction, and they are the fastest-growing structural materials in vehicles manufactured in the world [1]. The metallurgical and mechanical characteristics of these materials, i.e., chemical composition, microstructure, strength, toughness, formability, etc., allow the manufacturing of automotive components with weight reduction (by decreasing the thickness of strips) while still meeting safety demands and offering low cost and recyclability. Among AHSS, the most common is the dual-phase (DP) steel, whose microstructure is mainly composed of martensite particles scattered in a ductile ferrite matrix as a result of specific thermal treatments [2–4]. The mechanical strength and ductility level of these steel grades are mainly associated with the amount of martensite and ferrite in the microstructure, respectively [5–9]. These microstructural characteristics allow the manufacture of steel components with an excellent

combination of mechanical properties [10,11]. Recently, several studies have emerged related to corrosion resistance, microstructure prediction and effect of chemical composition and heat treatments in advanced DP steels [12–15]. One of the most important advantages of DP steel is that it can be produced with a low yield strength (*YS*)/tensile strength (*TS*) ratio (less than 0.70), making it ideal for a wide range of automotive components [16,17]. However, the main benefits and mechanical advantages of applying DP steels are highly dependent on the optimal design of the heat treatment cycles to obtain the desired mechanical properties. In general, the processing of cold rolled DP steels in industrial lines consists of an annealing heat treatment that involves partial or intercritical austenitization followed by rapid cooling to room temperature to get the dual-phase ferrite–martensite microstructure. Alternatively, to obtain galvanized sheets to improve the corrosion resistance of steel components, an interrupted cooling step is incorporated for the zinc coating stage [18–20]. This coating technique is the most effective and economic industrial process used to prevent corrosion, which consists in dipping the steel sheets in a molten zinc bath at temperatures around 460 °C. In industrial continuous galvanizing lines (CGL), cold rolled steel sheets are processed using a heat treatment that involves intercritical austenitization, controlled rapid cooling at the galvanizing temperature (460 °C), holding at this temperature for a few seconds, and finally rapid cooling at room temperature. The result of this complex thermal cycle should be a ferritic–martensitic microstructure [21,22]. In this regard, Liu et al. [23] evaluated the influence of CGL thermal parameters on microstructure and mechanical properties of DP steel showing that the most important processing parameters to manufacturing hot-dip GDP steels are the intercritical annealing temperature (*IAT*), intercritical annealing time (*IAt*), first cooling rate (*CR1*), isothermal holding time at the galvanizing temperature (*tg*) and the second cooling rate up to room temperature (*CR2*). The final microstructure of steel is quite sensitive to each operational parameter. Slight variations in the processing variables may result in important changes in the amount, size and distribution of the ferrite–martensite mixture and consequently alter the resulting mechanical properties of GDP steels [24–26]. Therefore, each heat treatment variable involved must be correctly selected to satisfy the mechanical properties. A number of research works have been reported dealing with the prediction of mechanical properties of DP steels using numerical methods based in diffusion equations, morphology and microstructural characteristics [27,28]. Furthermore, several approaches have been taken to study the outcome on the obtained mechanical and microstructure properties when the corresponding process parameters are modified [25,26]. In the design process for these materials a trial and error practice is common, which can be expensive if optimal configurations are sought; however, practical, useful and optimal configurations for the process parameters can be obtained with computational approaches in a less expensive manner. For example, a reasonable trade-off between accuracy and ease of calculation is achieved by the application of a two-level factorial design in combination with a complex iterative finite difference numerical approach for the one-dimensional heat transfer model in a sensitivity analysis of boron hot stamping steel [29].

As highlighted, the properties of interest in advanced DP steels are the yield strength (*YS*), ultimate tensile strength (*UTS*) and the percentage of elongation (*EL*). Due to the complex system nature of the steel properties relationship, non-linear models are used and implemented for the parameters evaluation for different configurations in the heat treatment processes design. Once the mentioned non-linear model is defined a DP steel with the best desired mechanical properties can be obtained if the controlled process parameters are optimally chosen. In the context of non-linear modeling for this kind of problem, artificial neural networks (ANNs) have been widely used to evaluate, predict and improve materials with their corresponding processes. In particular, when the ANN is trained using the back-propagation algorithm it is called a back-propagation artificial neural network (BPNN), and this process is explained in Section 2.1. Haque et al. [30] used an ANN to analyze corrosion-fatigue crack growth in DP steels. Back-propagation ANNs were also used by the same authors to predict fracture toughness and tensile strength in micro-alloyed

steels as a function of microstructure [31]. Chemical composition effects and intercritical heat treatment parameters on percentage of elongation and tensile strength of Si–Mn TRIP steels were modeled by Hosseini et al. [32] using a BPNN with a feed forward topology. Bustillo et al. [33] optimized the gap between a carbon steel sheet joined with an aluminum sheet by friction drilling process using machine learning techniques such as artificial neural networks, regression trees and ensembles of AdaBoost decision stumps. Bahrami et al. [34] used a neural network model to predict the mechanical properties of DP steels. Sterjovski et al. [35] applied ANNs to predict several mechanical properties such as hardness of affected zone, impact toughness, strength and hot ductility for different steel applications. Mechanical properties influenced by microstructural features, transition temperature, heat treatment conditions and alloying elements for high-strength DP steels were studied using artificial intelligence techniques by Krajewski and Nowacki [36]. Vafaeenezhad et al. [37] presented a soft computational approach in order to analyze the influence parameters in manufacturing DP steels using an ANN and adaptive neuro-fuzzy inference system (ANFIS). Buffa et al. [38] predicted mechanical and microstructural properties using an ANN coupled with an existing 3D FEM model in friction stir welding processes of DP titanium alloys. Recently, a hybrid strategy based in an ANN and genetic algorithm (GA) was applied to design DP steels in one-step thermal cycles with improved performance [39]. Thus, the good predictive behavior of an ANN when it is used to model non-linear phenomena, the well-known optimization performance of the multi-objective genetic algorithm (MOGA) and the fact that none of the mentioned research works has used a combined ANN and MOGA to design complex two-step heat treatments of hot-dip GDP steels are the main motivations and novel contributions of this paper in this field. Moreover, this work also represents a reference study using standard artificial intelligence and evolutive techniques like BPNN-MOGA to obtain reliable optimal results in comparison with the promising and recent metaheuristic optimization algorithm like the one already used and tested in a preceding publication [40].

Therefore, in this study a non-linear BPNN combined with a MOGA is applied simultaneously to determine the relationship between mechanical properties and continuous galvanizing parameters to define thermal cycle variables in an optimal manner to produce ultra-high-strength GDP steels with specific mechanical properties. The research is structured as follows: experimental methodology and computational procedures are described in Section 2, some numerical optimal results are obtained and discussed, as well as the corresponding experimental validation, in Section 3, followed by some conclusions in the last section.

2. Materials and Computational Method

The experimentally simulated thermal cycles to produce GDP steels were performed on experimental samples of a low carbon low alloy steel. The chemical composition of steel, which in fact is within the required technological ranges used to fabricate DP steels [17,18] resulting from the combustion method and optical spectrometry analysis, is presented in Table 1. The experimental material was treated in as-received condition, i.e., cold rolled sheets 1.1 mm thick.

Table 1. Composition (wt %) of the investigated steel.

Element	C	Si	Mn	P	S	Cr	Mo	Ni	B
wt %	0.154	0.260	1.906	0.013	0.0009	0.413	0.108	0.048	0.0010
Element	**Al**	**Cu**	**Nb**	**Ti**	**V**	**Ca**	**N**	**Fe + impurities**	
wt %	0.036	0.018	0.004	0.044	0.008	0.001	0.0036	Balance	

In Figure 1 the reproduced thermal cycles are outlined in detail, highlighting the processing variables studied (*CR1*, *tg* and *CR2*) and corresponding experimental ranges. The heat treatments thus designed were performed with a quenching dilatometer Linseis

model L78-RITA. In order to measure the mechanical properties, the designated thermal cycles were replicated on tension test sub-size specimens subjected to uniaxial tension tests. The applied experimental matrix is shown in detail in Table 2. The experimental data for this research were taken from [26]. The microstructural evolution during the heat treatments was first analyzed on the basis of the continuous cooling transformation (CCT) and time-temperature-transformation (TTT) diagrams theoretically calculated by means of JMatPro (Java-based Materials Properties). Furthermore, desired mechanical properties were obtained once the processing parameters were optimally found through the multi-objective genetic algorithm (MOGA) applied to the non-linear BPNN model.

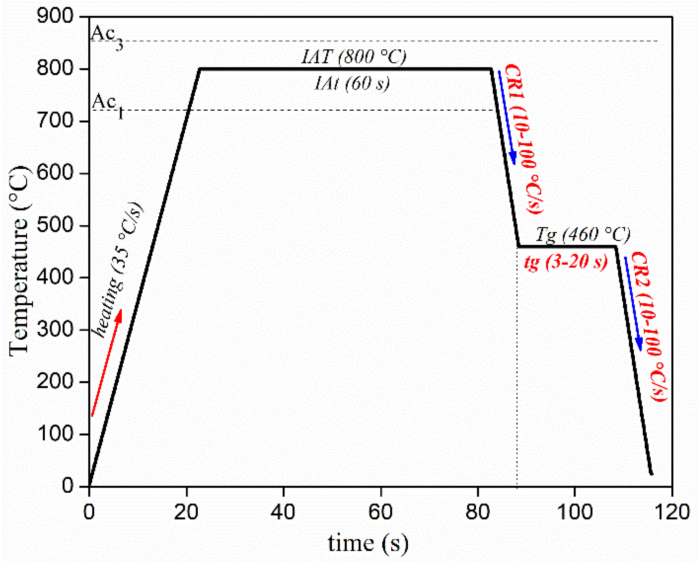

Figure 1. Graphic representation of the thermal cycles experimentally simulated by quenching dilatometry. The heat treatment variables studied (*CR1*, *tg* and *CR2*) and corresponding range are highlighted in the cooling profile, taken from [26].

Table 2. Resulting experimental matrix used in this research work [26].

Input Variables:							**Factor Level**	
							−1	**+1**
x_1, *CR1* (Cooling rate after intercritical austenitizing, °C/s)							10	110
x_2, *tg* (Holding time at the galvanizing temperature, s)							3	20
x_3, *CR2* (Cooling rate to room temperature, °C/s)							10	110
Output variables: *YS*, MPa (Yield strength, MPa)								
UTS, MPa (Ultimate tensile strength, MPa)								
EL, % (Total elongation)								
Sample	*CR1*, °C/s	*tg*, s	*CR2*, °C/s	*YS*, MPa	*UTS*, MPa	*EL*, %	*YS/UTS*	
1	30	17	90	729	1142	11.3	0.64	
2	10	11	60	754	1174	12.1	0.64	
3	110	11	60	829	1237	10.3	0.67	
4	60	11	60	853	1245	10.8	0.69	
5	90	6	30	890	1264	8.3	0.70	
6	60	11	10	745	1141	9.9	0.65	
7	30	17	30	725	1131	10.7	0.64	

Table 2. *Cont.*

Input Variables:							Factor Level	
							−1	+1
8	30	6	90	841	1226	8.6	0.69	
9	30	6	30	791	1196	9.8	0.66	
10	90	6	90	959	1274	8.6	0.75	
11	60	20	60	730	1123	9.9	0.65	
12	60	11	60	828	1187	10.5	0.70	
13	60	11	110	781	1203	10.7	0.65	
14	90	17	90	779	1145	9.4	0.68	
15	60	11	60	844	1199	9.5	0.70	
16	90	17	30	777	1166	10.1	0.67	
17	60	3	60	1015	1294	8.0	0.78	

2.1. Artificial Neural Network Modeling and Back-Propagation

The relationship among the mechanical properties and process parameters of GDP steels were modeled with the incorporation of an artificial neural network (ANN) due to its good behavior and numerical performance for complex systems. An ANN is defined by means of interconnected neurons where an input data point (Xi) is influenced by a weighted activation function. The ANN model performance depends on the entire layer structure that is formed by the arranged interconnected neurons. This layer structure can increase and improve the ANN performance, probably with a higher computational effort. Once the ANN model is defined it needs to be trained or it must learn from the measured experimental data. This is called the ANN learning process or training, and the back-propagation algorithm is used for this purpose, where two stages are usually involved. In the first phase a mean square error (MSE) is computed using the ANN response (Y_k) and the real experimental data (y_k) which read:

$$MSE = \frac{1}{n}\sum_{k=1}^{n}(Y_k - y_k)^2 \quad (1)$$

Once the MSE is computed, the weights in the hidden layers of the ANN model must be modified in a smart way in order to reduce the MSE. In fact, this becomes an optimization problem where the minimum of MSE as the objective function must be reached. The Levenberg–Marquardt algorithm is typically used to solve such problem. In this work the defined ANN architecture was of the form 3-9-9-3 and it is depicted in Figure 2. The ANN model was implemented in MATLAB. The reported ANN structure was chosen in this manner since it provided the best fitting among several tested configurations. The hyperbolic tangent sigmoid function was used as activation function, 48 epochs were needed to reach a training performance of 43.0639 with a corresponding gradient value of 1.0047 $\times$ 10^{-8}. Furthermore, a comparison between the ANN output responses and the real experimental data is reported in Figure 3, where an excellent performance of the BPNN trained model is observed. Thus, the computed BPNN model was successfully used to predict the galvanizing process in advanced DP steels.

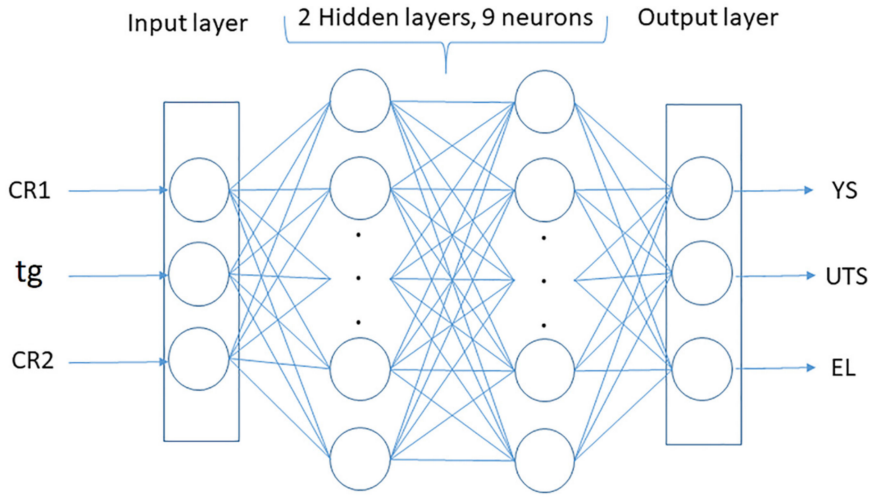

Figure 2. Configuration of the artificial neural network (ANN) model.

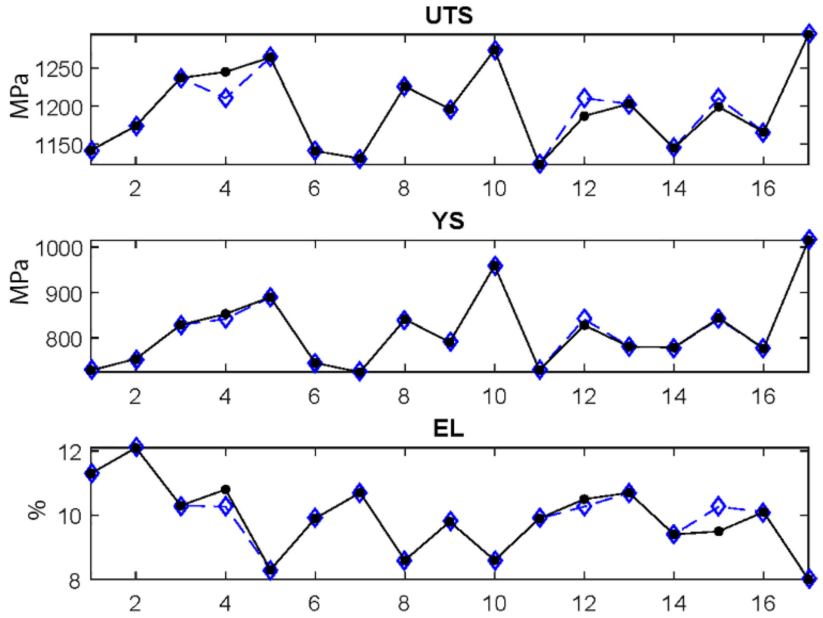

Figure 3. Back-propagation artificial neural network (BPNN) trained model validation. Experimental data (dot-continuous line) and ANN predicted values (diamond-dashed line).

2.2. Multi-Objective Optimization Problem

A multi-objective optimization problem must be defined, in particular, a three objective function should be stated when the following three mechanical properties are under consideration: *UTS*, *YS* and *EL*. Furthermore, some restrictions should also be imposed. The first conditions are directly related to the *UTS*, which is expected to reach a minimum value of 1100 MPa. A second restriction is over the *YS*, which must fall into the following range (550–750 MPa). Finally, the last restriction is extracted from *EL*, which should be at least 10%. Under this setting it is expected to obtain the best thermal cycles for the GDP steels design. Considering this, the following optimization problem is formally stated:

$$min(-f_1(x),\ f_2(x) - f_3(x)) \tag{2}$$

subject to:

$$10 \leq x_1 \leq 110 \tag{3}$$

$$10 \leq x_2 \leq 110 \tag{4}$$

$$3 \leq x_3 \leq 20 \quad (5)$$

where x_1, x_2 and x_3 denote cooling rate 1 (CR_1), cooling rate 2 (CR_2) and holding time at the galvanizing temperature (tg), respectively. The non-linear output of the BPNN model is a vectorial function written as $f(x) = (f_1(x), f_2(x), f_3(x))$, where $f_1(x)$, $f_2(x)$ and $f_3(x)$ refer to *UTS*, *YS* and *EL*, respectively. Once the multi-objective optimization is completely defined, it is numerically solved with a standard genetic algorithm, in this case the well-known nondominated sorting genetic algorithm was applied [41]. This algorithm found better fitness values with an elitist and controlled strategy that helped to increase the diversity of the population. The closeness among individuals was measured using the crowding distance and the concept of spread, which measured the movement of the Pareto front set used as a stopping condition. Thus, the computed solutions on the Pareto front were spread evenly, and the extreme objective function values did not change significantly with respect to the algorithm iterations when the spread was small. Desired mechanical properties can be obtained once optimal solutions are extracted from the computed Pareto front.

3. Results and Discussion

3.1. Influence of the Heat Treatment Variables

The resulting mechanical properties are individually analyzed in Figure 4. The relationships between *YS* and the thermal cycle variables including *CR1*, *tg* and *CR2* are shown on a surface plot in Figure 4a–c. It can be seen in a generalized way that increasing *CR1* was conducive to an increase in *YS* (Figure 4a,b), principally for small values of *tg* at the galvanizing temperature (460 °C). *YS* decreased as the *tg* increased. Independent of the cooling rates (Figure 4a,b), the highest *YS* was achieved at short *tg*. *CR2* appeared to have no significant effect over *YS* (Figure 4b,c). The behavior between *UTS* and the thermal cycle variables are shown on Figure 4d–f. Like *YS*, Figure 4d,f reveals that *UTS* increased when the initial *CR1* also increased. Similarly, *UTS* tended to increase when *tg* decreased, which experimentally showed the stage of the hot-dip galvanizing process (Figure 4d,e). The maximum tensile strength was reached at high *CR1* and small holding times of *tg*. Finally, relationships between the elongation at fracture (*EL*) and the thermal cycle variables are exposed in Figure 4g–i. Unlike *YS* and *UTS*, it can be noted that *EL* directly related to the ductility of steel tended to decrease with increasing the first cooling rate (*CR1*) and reducing the time taken for the galvanizing process of steel (*tg*).

As reported [24–26], the influence of controlling variables of the thermal cycle on the final mechanical properties of GDP steels is directly related to the microstructure developed in each stage of heat treatment. In this regard, to sustain the relationships explained above between variables and responses, the CCT-TTT diagrams calculated for the steel investigated using JMatPro software are shown in Figure 5a,b. At the industrial level, these phase transformation diagrams are very important for the study and development of new steels. They are mainly used as a support tool to design thermal cycles and predict the microstructural and mechanical behavior of steel, as have been demonstrated by several authors for different types of advanced steels [42–44]. In particular, these graphical representations reveal the temperatures at which certain phase transformations start and end, generated as consequence of the non-isothermal and isothermal transformation process of austenite. In this special research, the study of the phases developed in the cooling ramps (*CR1* and *CR2*) and isothermal stage (*tg*) was completed by the TTT and CCT diagrams, respectively. Figure 5a reports the CCT diagram where the investigated cooling range for *CR1* (10–100 °C/s) in the first stage of heat treatment is superimposed in a solid red line up to 460 °C (typical galvanizing temperature). From this analysis, it is clear that applying the slower cooling rate (10 °C/s), the transformed phases would be proeutectoid ferrite, bainite and perhaps slight martensitic transformation, which coincide with the minor mechanical properties recorded. For higher cooling rates (30, 60 and 90 °C/s), the resulting phases would contain a combination of bainite and martensite, consistent with the improvement in mechanical properties manifested. Finally, according to the CCT diagram, by using the highest cooling rate (110 °C/s), there would be total martensitic transformation that corre-

sponds to the highest reported mechanical strength values. This analysis and correlation between phases and properties, fully coincides with previous research works [44–47].

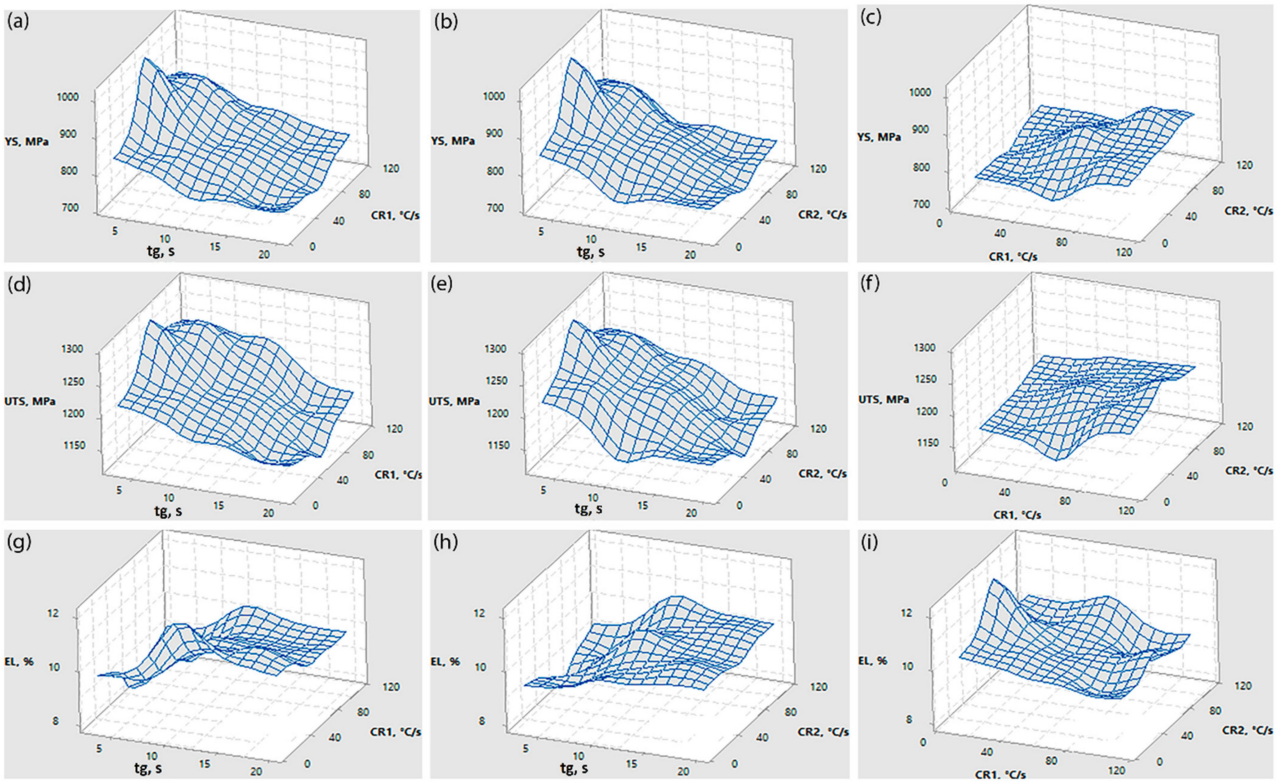

Figure 4. Relationships between yield strength (*YS*), ultimate tensile strength (*UTS*) and elongation at fracture (*EL*) and heat treatment parameters, including initial cooling rate (*CR1*), holding time at the galvanizing temperature (*tg*) and the final cooling rate to room temperature (*CR2*). (**a**) YS vs. tg and CR1, (**b**) YS vs. tg and CR2, (**c**) YS vs.tg CR1 and CR2, (**d**) UTS vs. tg and CR1, (**e**) UTS vs. tg and CR2, (**f**) UTS vs.tg CR1 and CR2, (**g**) EL vs. tg and CR1, (**h**) EL vs. tg and CR2, (**i**) EL vs.tg CR1 and CR2.

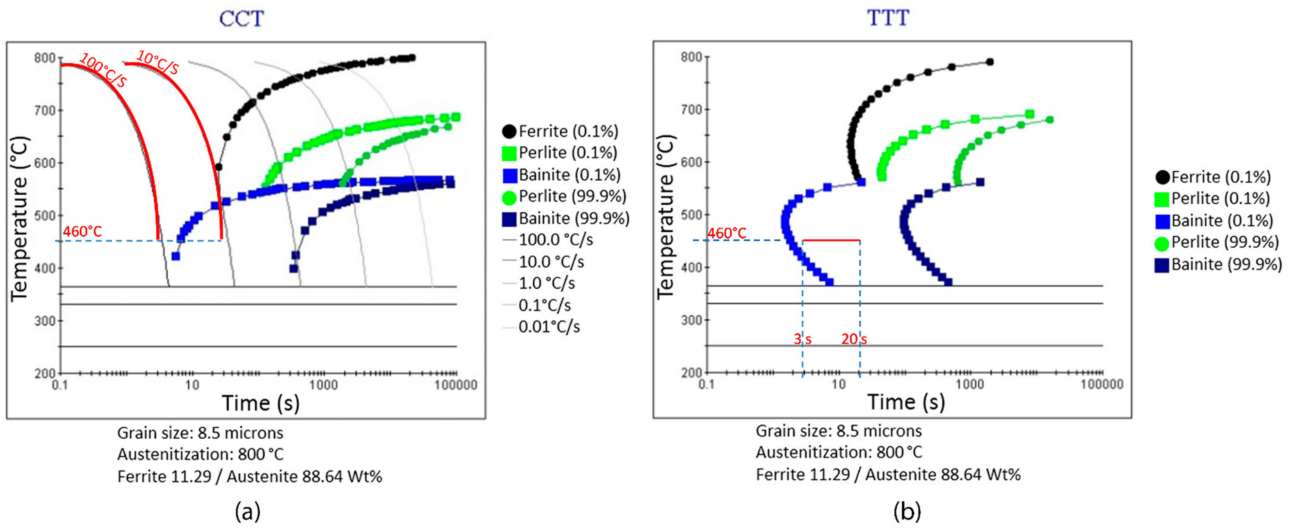

Figure 5. Phase transformation diagrams calculated by using JMatPro software. (**a**) Continuous cooling transformation (CCT) diagram and (**b**) time-temperature-transformation (TTT) diagram.

Similarly, the microstructural progress was analyzed in detail in the isothermal stage that simulates the galvanized step. For this purpose, the calculated TTT diagram (Figure 5b) was

used in which the selected time range (3–20 s) corresponding to the second experimental variable (*tg*) is highlighted (solid red line) at 460 °C. As can be noticed, this isothermal stage totally coincided with the isothermal bainite transformation, which reveals that the bainite existing in the final microstructure of steel depends directly on this parameter. It can be seen that prolonged holding times, i.e., long *tg*, led to a greater transformation of isothermal bainite and therefore less martensite. If the time in the isothermal stage is too long, the residual or remaining austenite can be totally consumed, resulting in a microstructure without martensite contents. The absence of martensite caused a notable decrease in YS and UTS. Similarly, recent research has reported [48] that the isothermal maintenance at 460 °C for the galvanizing process is considered the most critical stage of the thermal cycle since it can promote the transformation of isothermal bainite and/or stabilize the remaining austenite, which reduces the final mechanical properties of steel. In this critical stage of interrupted cooling, the concentration of alloying elements and particularly the carbon content of the residual austenite are dynamically varied. Due to this complicated microstructural evolution and metallurgical phenomena, there are still no phenomenological models that precisely describe this important microstructural and mechanical behavior. Finally, the analysis of the second cooling rate (*CR2*) corroborated that it did not alter the microstructure and the resulting mechanical properties in a significant manner. This behavior is mainly attributed to the fact that most of the possible phase transformations that control the final microstructure already occurred in the two previous stages. These results are consistent with previous studies that report minimal influence of *CR2* over the microstructure and obtained mechanical properties of DP steels [2,26]. It is clear then that the operational parameters of the continuous galvanizing annealing process significantly determine the mechanical properties of GDP steels. Therefore, it is necessary to establish the relationship among parameters, microstructure and properties to get the ideal configuration and optimize the manufacturing process in both research and industrial practice.

3.2. Optimization and Validation

As it was already mentioned in previous sections, the main purpose in this study related to the mechanical properties in order to maximize *UTS*, *EL* and minimize *YS*. In particular, a BPNN model and the nondominated sorting genetic algorithm (NSGA) were applied for the mathematical modeling and genetic optimization, respectively. The achieved total set of optimal solutions known as Pareto front set is reported in Table 3. The optimized values of heat treatment parameters and response variables were experimentally validated by selecting three characteristic thermal cycle conditions (run 7, 12 and 18) that entirely satisfied the previously established mechanical properties (550 < *YS* < 750 MPa, 1100 MPa < *UTS* and 10% < *EL*). The mechanical properties were measured from a tensile test on micro-tension specimens heat-treated in quenching dilatometry. In Figure 6 the obtained stress-strain curves are presented, which show the usual mechanical response to uniaxial tension of this kind of advanced steels (low elastic limit and yield strength values, high strain hardening, high ultimate strength and good elongation at fracture). The resulting values of *UTS* and *YS* were taken from the experimental curves; meanwhile, *EL* data was obtained from the fractured samples. Table 4 contains the results derived from the artificial intelligence and genetic optimization method and the experimental results. As can be seen in Figure 7 the results predicted and optimized by BPNN and GA fully coincided for the tree cases with the experimental results. Only small deviations were observed in the most critical cases, which should be taken as insignificant considering that they did not exceed 10%. When these results were compared with previous research conducted by this research group [26], it was noted that the prediction errors of the model used in the past work for the calculation of *YS* (error < 7.7%), *UTS* (error < 3.4%) and *EL* (error < 7.6%) were very similar to those found with the BPNN model in this research work. Although, it is very well known that any well-trained ANN-based model is superior to any other statistical approach due to the nature of the artificial neural network structures to model

non-linear phenomena. In fact, the use of artificial intelligence methods combined with genetic optimization allows solving the multi-objective optimization problem in a more practical and reliable way compared to the promising and recently proposed bio-inspired squirrels optimization algorithm studied in [40]. Considering this, the prediction error was significantly lower by the common application of artificial intelligence and genetic optimization with respect to the method based on a multi-objective metaheuristic approach using an adaptive memory procedure, MOAMP-squirrels search algorithm. It can be assumed that the best thermal cycle condition to manufacture an experimental DP1100 steel with the needed mechanical properties of 550 < *YS* < 750 MPa, 1100 MPa < *UTS* and 10% < *EL* was the heat treatment exposed in the run 18 because this experimental condition had the lower ratio *YS*/*UTS* desirable to achieve a greater plastic deformation necessary to produce complex automotive structural components. A *YS*/*UTS* ratio between 0.4–0.7 was reported for the cold rolled DP steel sheet to ensure a large formability range [18]. Based on the analysis and presented results it was corroborated that the non-linear BPNN model and NSGA algorithm simultaneously predicted with sufficient accuracy the mechanical properties behavior of GDP steels under galvanizing conditions.

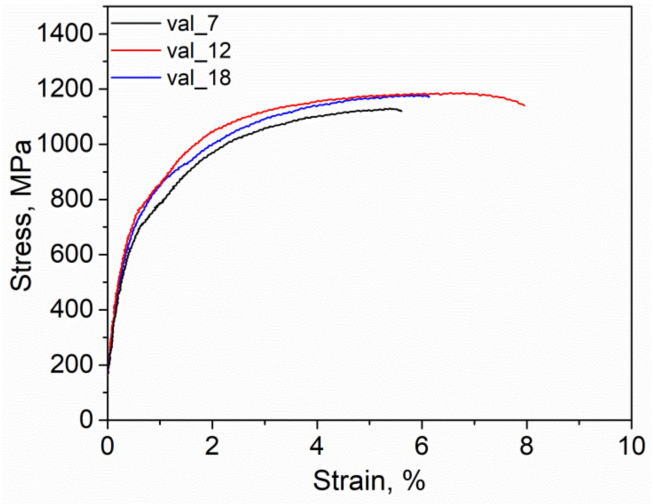

Figure 6. Stress-strain curves produced for the experimental validation of the proposed optimization program (run 7, 12 and 18).

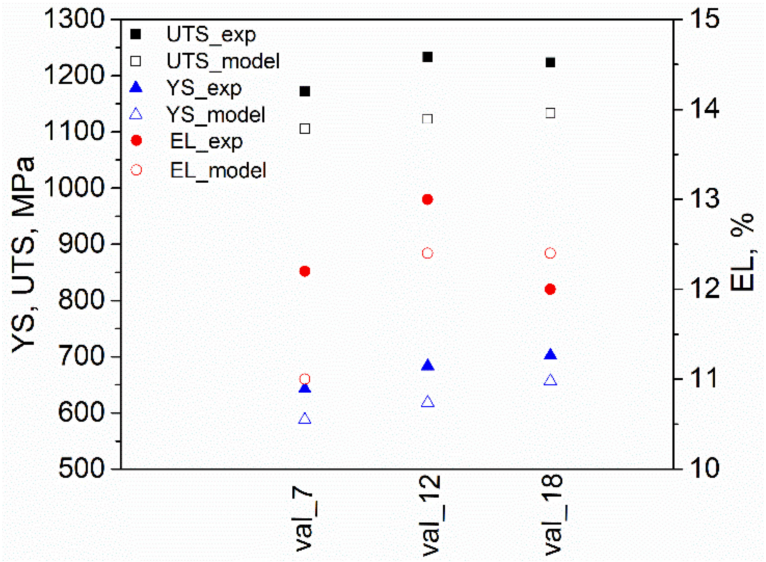

Figure 7. Comparison of predicted and experimental mechanical properties.

Table 3. Optimal Solutions. Thermal cycles for experimental validation (run 7, 12 and 18).

Run	*CR1*, °C/s	*tg*, s	*CR2*, °C/s	*UTS*, MPa	*YS*, MPa	*EL*, %	*YS*/*UTS*
1	10.00182	13.99614	34.77533	1106.142	588.0543	12.24872	0.531627
2	10.003	13.1638	51.73712	1134.372	680.616	13.35413	0.599994
3	99.31022	3.000085	45.95422	1349.958	1086.974	7.68546	0.805191
4	34.46106	4.357448	47.89058	1256.3	916.8248	9.554646	0.729782
5	31.79099	5.867405	54.15924	1265.731	934.1241	9.335757	0.738012
6	10.77097	10.76861	43.81834	1173.017	726.347	12.28939	0.619213
7	**15.42629**	**12.58661**	**44.08337**	**1133.863**	**656.6392**	**12.42769**	**0.579117**
8	22.28097	5.663389	46.01551	1226.594	845.2127	10.77376	0.689073
9	97.09112	5.962924	47.90645	1302.206	1037.868	8.639765	0.797008
10	27.98848	6.507693	44.33613	1230.357	864.0816	10.10007	0.702302
11	98.9381	3.002146	57.88625	1337.384	1118.232	7.940813	0.836133
12	**10.18243**	**12.29477**	**36.75881**	**1123.346**	**618.2115**	**12.45085**	**0.55033**
13	10.14282	11.96282	44.3358	1144.296	668.3764	12.84635	0.584094
14	40.52644	6.702923	53.91026	1272.773	976.1051	8.534069	0.766912
15	22.99108	6.11916	54.00259	1244.925	871.298	10.38634	0.69988
16	86.09068	3.267752	43.24556	1310.418	1017.792	7.544843	0.776692
17	12.45043	9.972871	45.30469	1191.887	767.8903	11.8921	0.644264
18	**10.00182**	**13.99614**	**34.77533**	**1106.142**	**588.0543**	**12.24872**	**0.531627**
19	12.98674	9.594106	39.9344	1184.483	757.5647	11.64299	0.639574
20	82.50954	3.51339	42.70804	1298.414	1000.026	7.539304	0.77019

Table 4. Results of genetic optimization compared to experimental results.

#Test	*CR1* (°C/s)	*tg* (s)	*CR2* (°C/s)	Model Results			Experimental Results			Error, %		
				UTS (MPa)	*YS* (MPa)	*EL* (%)	*UTS* (MPa)	*YS* (MPa)	*EL* (%)	*UTS*	*YS*	*EL*
Val_7	10	14	34.8	1106.1	588	12.2	1172	642.8	11	5.9	9.31	9.8
Val_12	10.18	12.3	36.8	1123.3	618.2	12.4	1233.2	683	13	9.7	9.9	4.8
Val_18	15.42	12.5	44	1133.9	656.7	12.4	1223.4	702.4	12	7.8	6.9	3.22

4. Conclusions

In the present research work, the relationship between continuous galvanizing variables and mechanical properties was successfully determined using a non-linear back-propagation neural network (BPNN) combined with a multi-objective genetic algorithm (MOGA). This is the first time that this computational approach was used to optimize complex two-step heat treatments involved in the continuous galvanizing process of DP steels. In fact, this work represents an improved and forward step with respect to the response surface methodology approach previously presented. So, the main conclusions of this research work are:

1. The prediction error is lower with the common application of artificial intelligence and genetic optimization compared to the biological-inspired optimization algorithm. Thus, the obtained non-lineal model using an ANN showed excellent prediction of mechanical properties for GDP steel processed under continuous galvanizing conditions with a prediction error less than 10%.

2. It was verified that the most significant heat treatment parameter on the final mechanical properties during the experimental continuous galvanizing process of DP steels is the isothermal holding time (*tg*) at the galvanizing temperature (460 °C).
3. Following the proposed computational methodology, hot-dip GDP steels with an extraordinary combination of mechanical properties (550 < *YS* < 750 MPa, 1100 MPa < *UTS* and 10% < *EL*) can be produced. The best combination of continuous galvanizing process parameters for this purpose may be: Heating of the sheet steel to the intercritical temperature region of 800 °C for 60 s, rapid cooling at 10 °C/s (*CR1*) to 460 °C, isothermal holding during 14 s (*tg*) and final quench at 35 °C/s (*CR2*).
4. This modeling and optimization study can be useful in real-world applications, particularly to optimal design of thermal cycles for practical processing of GDP steels.

Author Contributions: Conceptualization, E.O.R.-F. and G.A.-G.; Methodology, G.A.-G. and P.S.C.; Software, E.O.R.-F. and A.E.S.-R.; supervision, E.O.R.-F., A.S.-R. and F.G.; Validation, P.S.C.; Writing—original draft, E.O.R.-F. and G.A.-G.; Writing—review and editing, E.O.R.-F. and G.A-G. All authors have read and agreed to the published version of the manuscript.

Funding: This research received no external funding.

Data Availability Statement: Not applicable.

Acknowledgments: The authors would like to thank CINVESTAV (Unidad Saltillo) and the International Zinc Association (IZA) for the support and technical assistance in this research work.

Conflicts of Interest: The authors declare no conflict of interest.

References

1. Kuziak, R.; Kawalla, R.; Waengler, S. Advanced high strength steels for automotive industry. *Arch. Civ. Mech. Eng.* **2008**, *8*, 103–117. [CrossRef]
2. Fonstein, N. Main Features of Heat Treatment from Intercritical Region. In *Advanced High Strength Sheet Steels*; Springer International Publishing: Cham, Switzerland, 2015; pp. 17–65. [CrossRef]
3. Park, K.; Nishiyama, M.; Nakada, N.; Tsuchiyama, T.; Takaki, S. Effect of the martensite distribution on the strain hardening and ductile fracture behaviors in dual-phase steel. *Mater. Sci. Eng. A* **2014**, *604*, 135–141. [CrossRef]
4. Yi, J.J.; Yu, K.J.; Kim, I.S.; Kim, S.J. Role of retained austenite on the deformation of an Fe-0.07 C-1.8 Mn-1.4 Si dual-phase steel. *Met. Mater. Trans. A* **1983**, *14*, 1497–1504. [CrossRef]
5. Sugimoto, K.-I.; Misu, M.; Kobayashi, M.; Shirasawa, H. Effects of Second Phase Morphology on RetainedAustenite Morphology and Tensile Properties in a TRIP-aided Dual-phase Steel Sheet. *ISIJ Int.* **1993**, *33*, 775–782. [CrossRef]
6. Sun, S.; Pugh, M. Properties of thermomechanically processed dual-phase steels containing fibrous martensite. *Mater. Sci. Eng. A* **2002**, *335*, 298–308. [CrossRef]
7. Rashid, M.S. Dual Phase Steels. *Annu. Rev. Mater. Res.* **1981**, *11*, 245–266. [CrossRef]
8. Granbom, Y. Effects of Process Parameters prior to Annealing on the Formability of Two Cold Rolled Dual Phase Steels. *Steel Res. Int.* **2008**, *79*, 297–305. [CrossRef]
9. Allain, S.; Bouaziz, O.; Pushkareva, I.; Scott, C. Towards the microstructure design of DP steels: A generic size-sensitive mean-field mechanical model. *Mater. Sci. Eng. A* **2015**, *637*, 222–234. [CrossRef]
10. Waterschoot, T.; De Cooman, B.C.; De, A.K.; Vandeputte, S. Static strain aging phenomena in cold-rolled dual-phase steels. *Met. Mater. Trans. A* **2003**, *34*, 781–791. [CrossRef]
11. Ghassemi-Armaki, H.; Maaß, R.; Bhat, S.; Sriram, S.; Greer, J.; Kumar, K. Deformation response of ferrite and martensite in a dual-phase steel. *Acta Mater.* **2014**, *62*, 197–211. [CrossRef]
12. Park, I.-J.; Kim, S.-T.; Lee, I.-S.; Park, Y.-S.; Moon, M.B. A Study on Corrosion Behavior of DP-Type and TRIP-Type Cold Rolled Steel Sheet. *Mater. Trans.* **2009**, *50*, 1440–1447. [CrossRef]
13. Aslam, I.; Li, B.; Martens, R.; Goodwin, J.; Rhee, H.; Goodwin, F. Transmission electron microscopy characterization of the interfacial structure of a galvanized dual-phase steel. *Mater. Charact.* **2016**, *120*, 63–68. [CrossRef]
14. Sodjit, S.; Uthaisangsuk, V. Microstructure based prediction of strain hardening behavior of dual phase steels. *Mater. Des.* **2012**, *41*, 370–379. [CrossRef]
15. Ebrahimian, A.; Banadkouki, S.G. Effect of alloying element partitioning on ferrite hardening in a low alloy ferrite-martensite dual phase steel. *Mater. Sci. Eng. A* **2016**, *677*, 281–289. [CrossRef]
16. Flaxa, V.; Shaw, J. *Material Applications in ULSAB-AVC (Advanced Vehicle Concepts)*; SAE Technical Paper Series 2002-01-2074; SAE International: Warrendale, PA, USA, 2002.
17. Schmitt, J.-H.; Iung, T. New developments of advanced high-strength steels for automotive applications. *Comptes Rendus Phys.* **2018**, *19*, 641–656. [CrossRef]

18. Jamwal, R.S.; Frimpong, J.; Ehrhardt, B.W.; Bracht, H.V.; Boggs, R.D.; Bevans, S.W. Process for Making Cold-Rolled Dual Phase Steel Sheet. U.S. Patent 20,140,166,163 A1, 19 June 2014.
19. Movahed, P.; Kolahgar, S.; Marashi, S.; Pouranvari, M.; Parvin, N. The effect of intercritical heat treatment temperature on the tensile properties and work hardening behavior of ferrite–martensite dual phase steel sheets. *Mater. Sci. Eng. A* **2009**, *518*, 1–6. [CrossRef]
20. Mohanty, R.R.; Girina, O.A.; Fonstein, N.M. Effect of Heating Rate on the Austenite Formation in Low-Carbon High-Strength Steels Annealed in the Intercritical Region. *Met. Mater. Trans. A* **2011**, *42*, 3680–3690. [CrossRef]
21. Khondker, R.; Mertens, A.; McDermid, J. Effect of annealing atmosphere on the galvanizing behavior of a dual-phase steel. *Mater. Sci. Eng. A* **2007**, *463*, 157–165. [CrossRef]
22. Alibeigi, S.; Kavitha, R.; Meguerian, R.; McDermid, J. Reactive wetting of high Mn steels during continuous hot-dip galvanizing. *Acta Mater.* **2011**, *59*, 3537–3549. [CrossRef]
23. Liu, H.; Li, F.; Shi, W.; Swaminathan, S.; He, Y.; Rohwerder, M.; Li, L. Challenges in hot-dip galvanizing of high strength dual phase steel: Surface selective oxidation and mechanical property degradation. *Surf. Coat. Technol.* **2012**, *206*, 3428–3436. [CrossRef]
24. Pan, E.; Di, H.; Jiang, G.; Bao, C. Effect of Heat Treatment on Microstructures and Mechanical Properties of Hot-Dip Galvanized DP Steels. *Acta Met. Sin. (Engl. Lett.)* **2014**, *27*, 469–475. [CrossRef]
25. Kim, S.-J.; Cho, Y.-G.; Oh, C.-S.; Kim, D.E.; Moon, M.B.; Han, H.N. Development of a dual phase steel using orthogonal design method. *Mater. Des.* **2009**, *30*, 1251–1257. [CrossRef]
26. Costa, P.; Altamirano, G.; Salinas, A.; González-González, D.S.; Goodwin, F. Optimization of the Continuous Galvanizing Heat Treatment Process in Ultra-High Strength Dual Phase Steels Using a Multivariate Model. *Metals* **2019**, *9*, 703. [CrossRef]
27. Pernach, M.; Bzowski, K.; Pietrzyk, M. Numerical modeling of phase transformation in dual phase (DP) steel after hot rolling and laminar cooling. *Int. J. Multiscale Comput. Eng.* **2014**, *12*, 397–410. [CrossRef]
28. Bzowski, K.; Rauch, L.; Pietrzyk, M. Application of statistical representation of the microstructure to modeling of phase transformations in DP steels by solution of the diffusion equation. *Procedia Manuf.* **2018**, *15*, 1847–1855. [CrossRef]
29. Fernández, B.; González, B.; Artola, G.; De Lacalle, N.L.; Angulo, C. A Quick Cycle Time Sensitivity Analysis of Boron Steel Hot Stamping. *Metals* **2019**, *9*, 235. [CrossRef]
30. Haque, M. Prediction of corrosion–fatigue behavior of DP steel through artificial neural network. *Int. J. Fatigue* **2001**, *23*, 1–4. [CrossRef]
31. Haque, M. ANN back-propagation prediction model for fracture toughness in microalloy steel. *Int. J. Fatigue* **2002**, *24*, 1003–1010. [CrossRef]
32. Hosseini, S.; Zarei-Hanzaki, A.; Panah, M.Y.; Yue, S. ANN model for prediction of the effects of composition and process parameters on tensile strength and percent elongation of Si–Mn TRIP steels. *Mater. Sci. Eng. A* **2004**, *374*, 122–128. [CrossRef]
33. Bustillo, A.; Urbikain, G.; Perez, J.M.; Pereira, O.M.; de Lacalle, L.N.L. Smart optimization of a friction-drilling process based on boosting ensembles. *J. Manuf. Syst.* **2018**, *48*, 108–121. [CrossRef]
34. Bahrami, A.; Anijdan, S.M.; Ekrami, A. Prediction of mechanical properties of DP steels using neural network model. *J. Alloys Compd.* **2005**, *392*, 177–182. [CrossRef]
35. Sterjovski, Z.; Nolan, D.; Carpenter, K.; Dunne, D.; Norrish, J. Artificial neural networks for modelling the mechanical properties of steels in various applications. *J. Mater. Process. Technol.* **2005**, *170*, 536–544. [CrossRef]
36. Krajewski, S.; Nowacki, J. Dual-phase steels microstructure and properties consideration based on artificial intelligence techniques. *Arch. Civ. Mech. Eng.* **2014**, *14*, 278–286. [CrossRef]
37. Vafaeenezhad, H.; Ghanei, S.; Seyedein, S.H.; Beygi, H.; Mazinani, M. Process Control Strategies for Dual-Phase Steel Manufacturing Using ANN and ANFIS. *J. Mater. Eng. Perform.* **2014**, *23*, 3975–3983. [CrossRef]
38. Buffa, G.; Fratini, L.; Micari, F. Mechanical and microstructural properties prediction by artificial neural networks in FSW processes of dual phase titanium alloys. *J. Manuf. Process.* **2012**, *14*, 289–296. [CrossRef]
39. Dutta, T.; Dey, S.; Datta, S.; Das, D. Designing dual-phase steels with improved performance using ANN and GA in tandem. *Comput. Mater. Sci.* **2019**, *157*, 6–16. [CrossRef]
40. Altamirano-Guerrero, G.; García-Calvillo, I.D.; Reséndiz-Flores, E.O.; Costa, P.; Salinas-Rodríguez, A.; Goodwin, F. Intelligent design in continuous galvanizing process for advanced ultra-high-strength dual-phase steels using back-propagation artificial neural networks and MOAMP-Squirrels search algorithm. *Int. J. Adv. Manuf. Technol.* **2020**, *110*, 2619–2630. [CrossRef]
41. Deb, K.; Pratap, A.; Agarwal, S.; Meyarivan, T. A fast and elitist multiobjective genetic algorithm: NSGA-II. *IEEE Trans. Evol. Comput.* **2002**, *6*, 182–197. [CrossRef]
42. Cota, A.; Modenesi, P.; Barbosa, R.; Santos, D. Determination of CCT diagrams by thermal analysis of an HSLA bainitic steel submitted to thermomechanical treatment. *Scr. Mater.* **1998**, *40*, 165–169. [CrossRef]
43. You, W.; Xu, W.-H.; Liu, Y.-X.; Bai, B.-Z.; Fang, H.-S. Effect of Chromium on CCT Diagrams of Novel Air-Cooled Bainite Steels Analyzed by Neural Network. *J. Iron Steel Res. Int.* **2007**, *14*, 39–42. [CrossRef]
44. Bräutigam-Matus, K.; Altamirano, G.; Salinas, A.; Flores, A.; Goodwin, F. Experimental Determination of Continuous Cooling Transformation (CCT) Diagrams for Dual-Phase Steels from the Intercritical Temperature Range. *Metals* **2018**, *8*, 674. [CrossRef]
45. Kuang, S.; Kang, Y.-L.; Yu, H.; Liu, R.-D. Effect of continuous annealing parameters on the mechanical properties and microstructures of a cold rolled dual phase steel. *Int. J. Miner. Met. Mater.* **2009**, *16*, 159–164. [CrossRef]

46. Hüseyin, A.; Havva, K.Z.; Ceylan, K. Effect of intercritical annealing parameters on dual phase behavior of commercial low-alloyed steels. *J. Iron Steel Res. Int.* **2010**, *17*, 73–78. [CrossRef]
47. Calcagnotto, M.; Ponge, D.; Raabe, D. Microstructure Control during Fabrication of Ultrafine Grained Dual-phase Steel: Characterization and Effect of Intercritical Annealing Parameters. *ISIJ Int.* **2012**, *52*, 874–883. [CrossRef]
48. Wu, R.; Wang, L.; Jin, X. Thermal Stability of Austenite and Properties of Quenching & Partitioning (Q&P) Treated AHSS. *Phys. Procedia* **2013**, *50*, 8–12. [CrossRef]